

Article

# MHD Steady/Unsteady Porous Boundary Layer of Cu–Water Nanofluid with Micropolar Effect over a Permeable Surface

Kamal Raslan <sup>1</sup>, Selim Mohamadain <sup>2</sup>, Mohamed Abdel-wahed <sup>3,\*</sup>  and  
Elsayed M. Abedel-aal <sup>1,\*</sup>

<sup>1</sup> Mathematics Department, Faculty of Science, Al-azhar University, Cairo 002, Egypt;  
Kamal.Raslan@gmail.com

<sup>2</sup> Mathematics Department, Faculty of Science, Tanta University, Tanta 002, Egypt; mody\_mido\_100@live.com

<sup>3</sup> Basic Science Department, Faculty of Engineering, Benha University, Cairo 002, Egypt

\* Correspondence: eng\_moh\_sayed@live.com (M.A.); sayed\_12\_72@yahoo.com (E.M.A.);  
Tel.: +02-010-6886-0534 (M.A.); +02-011-2295-1473 (E.M.A.)

Received: 5 March 2018; Accepted: 3 April 2018; Published: 7 May 2018



**Abstract:** This work provides a mathematical model for the cooling process of a moving surface, in the presence of a uniform external magnetic field and thermal radiation, through a porous medium by using a weak concentration micropolar nanofluid. The model—based on the conservation equations of the unsteady case in the momentum and thermal boundary layer—takes into consideration the effect of the suction process. The conservation equations were transformed into ordinary differential equations using similar transformation techniques. The equations were solved numerically for the general case and analytically for the steady case. The rate of heat transfer, couple shear stress, and surface shear stress are deduced. We discuss the impact of these physical characteristics on the mechanical properties of the surface that will be cooled.

**Keywords:** nanofluids; micropolar; cooling process; mechanical properties

## 1. Introduction

We enhanced the thermal conductivity of the coolant based on its essential effects on many engineering applications, such as the heat treatment of metals [1]. The aim of the cooling process is to improve the metals' mechanical properties, such as ductility and strength. Creating more useful metals is one of the most important aims of researchers. In this process, the metal is heated to a certain temperature and then cooled in a series of specific operations. Nanofluids have properties that make them useful in many heat transfer applications, such as microelectronics, fuel cells, pharmaceutical processes, hybrid powered engines, engine cooling/vehicle thermal management, domestic refrigerators, heat exchangers, and the reduction of flue gas temperature in boilers [2]. Compared to the base fluid, thermal conductivity and the convective heat transfer coefficient were enhanced. In 1995, the authors of [3] proposed the idea of enhancing the thermal conductivity of the fluids using these nanoparticles. This was the first push for researchers to conduct studies that investigated the effects of nanoparticle types, sizes, and concentrations on the heat transfer characteristics and took into consideration some of the effects such as the thermal radiation, variable heat flux, magnetic field, and suction/injection processes [4]. We studied the magnetohydrodynamics (MHD) free convection of Al<sub>2</sub>O<sub>3</sub>–water nanofluid by considering the thermal radiation problem [5]. This study examined the flow and heat transfer over an unsteady shrinking sheet with suction in nanofluids [6]. The natural convection flow of a nanofluid over a linear stretching sheet, in the presence of a magnetic field, was discussed [7]. The mixed convection boundary layer flow from a horizontal

circular cylinder was embedded in a porous medium, which was filled with a nanofluid [8]. We observed the boundary layer flow over a stretching/shrinking surface under an external uniform shear flow with a convective surface boundary condition in a nanofluid [9]. The effect of a magnetic field on the flow and heat transfer of a nanofluid over an unsteady continuous moving surface—and in the presence of suction/injection—was observed [10]. Buongiorno's model was used to study the heat and mass transfer flow in a thin nanofluid film over an unsteady stretching sheet [11]. The study focused on the effects of thermophoresis and Brownian motion on the boundary layer flow of a nanofluid in the presence of thermal stratification—due to solar energy [12]. The flow and heat elements are transferred, in a nanofluid, over a moving surface with a non-linear velocity and variable thickness and in the presence of thermal radiation [13]. The boundary layer flow was maneuvered over a moving surface, which was embedded into a nanofluid, in the presence of a magnetic field and suction/injection [14]. We analyzed the effects of thermal radiation and heat generation on the mechanical properties of an unsteady, continuously moving cylinder in a nanofluid in the presence of suction/injection [15]. The flow and heat transfer was observed over a moving surface in a nanofluid with a non-linear velocity and variable thickness and in the presence of Brownian motion.

Micropolar fluids may represent fluids that consist of rigid, randomly oriented (or spherical) particles that are suspended in a viscous medium, where the deformation of fluid particles is ignored. The microrotation of the suspended microparticles within the fluid is discussed through the theory of micropolar fluids. In this theory, the fluids can be subjected to the surface and body couples, in which the material points in the volume elements can both move around the centers of mass and deform. Many researchers, such as the authors of [16], have investigated the micropolar fluid theory by studying the behavior of the unsteady boundary layer flow of a micropolar fluid near the rear stagnation point of a plane surface [17]. The unsteady mixed convection boundary flow of a micropolar fluid with uniform suction/injection over a stretching/shrinking sheet was analyzed [18]. We investigated the flow and heat transfer in a micropolar fluid along a stretching surface. According to the authors of [19], the effect of the thermal radiation interaction of the boundary layer flow of a micropolar fluid along a heated plate was embedded in a porous medium with variable heat flux [20]. The effect of variable heat flux on the heat transfer characteristics of a stretching surface in micropolar fluids was studied [21]. This study examined the influence of suction/injection and heat generation on the MHD flow of a micropolar fluid along a stretched permeable surface [22]. The heat transfer characteristic of a micropolar fluid along a heated vertical porous plate with variable suction and heat flux was compared to the Newtonian fluid [23]. The effects of the thermal radiation and heat generation were observed with respect to the flow and heat transfer characteristics over an unsteady moving surface in a micropolar fluid in the presence of suction/injection [24]. The suction/injection effects were studied on the micropolar fluid flow along a continuously moving plate in the presence of radiation [25]. The effects of microrotation and nanoparticle volumetric fraction on the fluid flow and heat transfer behavior in the boundary layer were observed [26]. We studied the effect of the microrotation of nanoparticles on the momentum boundary layer of a permeable stretching sheet in micropolar nanofluids with suction [27]. The flow and heat transfer of a micropolar fluid on a porous stretching sheet was observed [28]. The study recorded the effects of Soret and the non-uniform heat source/sink on the MHD non-Darcian convective flow along a stretching sheet in a micropolar fluid with the radiation effect [29]. We examined the effects of radiative and Joule heating on the MHD flow of a micropolar fluid with a partial slip and convective boundary condition problem [30], as well as on the micropolar nanofluid flow with MHD and viscous dissipation effects towards a stretching sheet with a multimedia feature [31]. We used the Chebyshev Spectral Newton Iterative Scheme to analyze the hydromagnetic Hiemenz flow of a micropolar fluid over a non-linear stretching/shrinking sheet [32], and investigated the MHD orthogonal stagnation-point flow of a micropolar fluid in the presence of a magnetic field that is parallel to the velocity at infinity [33]. The Lorentz force effect was observed on a mixed convection micropolar flow in a vertical conduit [34], along with the flow and heat transfer of a weak concentration micropolar nanofluid over a steady/unsteady moving surface [35]. The Molecular Dynamics Study

of Thermodynamic Properties of Nanoclusters for Additive Manufacturing was considered [36]. We observed the nanoscale liquid film that was sheared between strong wetting surfaces and studied the effects of the interface region on the flow [37], as well as the molecular dynamics simulations of oscillatory Couette flows with slip boundary conditions [38]. Viscous heating in the nanoscale shear driven liquid flows, as well as [39] the molecular dynamics of bimetallic nanoparticles—including the case of AuxCuy alloy clusters [40]—was studied. The thermal resistance at a liquid–solid interface, which is dependent on the ratio of thermal oscillation frequencies, along with [41] the molecular simulation of thermal transport across hydrophilic interfaces, was examined.

This work presents an investigation of the effect of microrotation of the nanoparticles along a moving plate, with time-dependent velocity and temperature, through a boundary layer that is subjected to thermal radiation and a suction process, in the presence of a uniform magnetic field through a porous medium. The study considered two cases, namely the steady weak concentration—which was solved analytically using the hypergeometric function—and the unsteady motion—which was solved numerically.

### 2. Formulation of the Problem

The study analyzed a steady/unsteady flow of an incompressible micropolar nanofluid over a permeable moving surface under the effect of thermal radiation with heat flux  $q_r$  and uniform suction  $S_w$ . This was analyzed in the presence of thermal radiation and a uniform magnetic field of strength  $B_0$  through a porous medium. The temperature of the outer surface is  $T_w$ , while  $T_\infty$  is the temperature of the free stream that is far away from the surface (see Figure 1). It is assumed that the nanoparticles have a uniform size and shape. In addition, both the fluid phase and the nanoparticles are assumed to be in thermal equilibrium state. The nanoparticles are also assumed to be very small in size, which means that the slip velocity between the phases is presumed to be negligible. The conservation equations for the unsteady micropolar nanofluid flow are presented below [23,26].

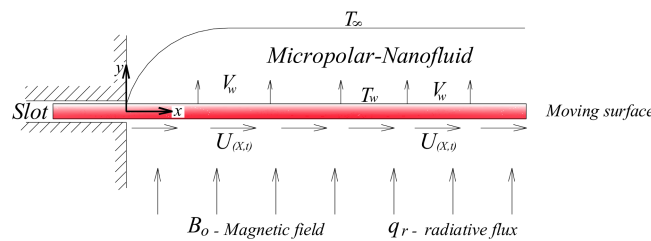


Figure 1. Physical model and coordinate system.

$$\frac{\partial u}{\partial x} + \frac{\partial v}{\partial y} = 0, \tag{1}$$

$$\frac{\partial u}{\partial t} + u \frac{\partial u}{\partial x} + v \frac{\partial u}{\partial y} = \left( \frac{\mu_{nf} + k^*}{\rho_{nf}} \right) \frac{\partial^2 u}{\partial y^2} + \frac{k^*}{\rho_{nf}} \frac{\partial \omega}{\partial y} - \frac{v}{K_p} u - \frac{\sigma B^2}{\rho} u, \tag{2}$$

$$\frac{\partial \omega}{\partial t} + u \frac{\partial \omega}{\partial x} + v \frac{\partial \omega}{\partial y} = \frac{\gamma_{nf}}{(\rho_{nf})_j} \frac{\partial^2 \omega}{\partial y^2} - \frac{k^*}{(\rho_{nf})_j} (2\omega + \frac{\partial u}{\partial y}), \text{ and} \tag{3}$$

$$\frac{\partial T}{\partial t} + u \frac{\partial T}{\partial x} + v \frac{\partial T}{\partial y} = \alpha_{nf} \frac{\partial^2 T}{\partial y^2} - \frac{1}{(\rho C_p)_{nf}} \frac{\partial q}{\partial y}. \tag{4}$$

These equations are subjected to the following boundary conditions.

$$\begin{aligned} u = U_w, v = S_w, T = T_w, \omega = -n \frac{\partial u}{\partial y} \text{ at } y = 0, \\ u \rightarrow 0, \omega \rightarrow 0, T = T_\infty \text{ as } y \rightarrow \infty, \end{aligned} \tag{5}$$

where  $n$  is the boundary parameter, with  $0 \leq n \leq 1$ . The case corresponds to  $n$  results in the vanishing of the anti-symmetric part of the stress tensor and represents a weak concentration. In this paper, this was the only case that was considered.

The spin gradient viscosity is defined below [34].

$$\gamma_{nf} = (\mu_{nf} + \frac{k^*}{2})j = \mu_f(\frac{1}{(1-\phi)^{2.5}} + \frac{K}{2})j. \tag{6}$$

The properties of the nanofluid are defined below [34] (see Table 1).

$$\begin{aligned} \mu_{nf} &= \left(\frac{\mu_f}{(1-\phi)^{2.5}}\right), \rho_{nf} = (1-\phi)\rho_f + \phi\rho_s, \alpha_{nf} = \frac{k_{nf}}{(\rho C_p)_{nf}}, \\ (\rho C_p)_{nf} &= (1-\phi)(\rho C_p)_f + \phi(\rho C_p)_s, \frac{k_{nf}}{k_f} = \frac{(k_s + 2k_f) - 2\phi(k_f - k_s)}{(k_s + 2k_f) + \phi(k_f - k_s)}. \end{aligned} \tag{7}$$

**Table 1.** Thermophysical properties of water and copper (Cu) [12].

Properties	Fluid (Water)	Cu
C <sub>p</sub> (J/kg K)	4179	385
Density (ρ) (kg/m <sup>3</sup> )	997.1	8933
Thermal conductivity (k) (W/m	0.613	400

Using Rosseland’s approximation for radiation, the radiative heat flux is simplified in Equation (8).

$$q_r = -\frac{4\sigma}{3 a^*} \frac{\partial T^4}{\partial y}. \tag{8}$$

Hence, by expanding  $T^4$  in a Taylor series about  $T_\infty$  and neglecting the higher order terms, we get Equation (9).

$$T^4 \cong 4TT_\infty^3 - 3T_\infty^4. \tag{9}$$

Using Equations (8) and (9) in the energy Equation (4), we get Equation (10).

$$\frac{\partial T}{\partial t} + u \frac{\partial T}{\partial x} + v \frac{\partial T}{\partial y} = \alpha_{nf} \frac{\partial^2 T}{\partial y^2} + \left(\frac{16\sigma T_\infty^3}{3\alpha(\rho C_p)_{nf}}\right) \frac{\partial^2 T}{\partial y^2}. \tag{10}$$

Assuming that the velocity and the fluid temperature are in the form below.

$$U_w(x, t) = \frac{bx}{1-\alpha t}, T_w(x, t) = T_\infty + \frac{cx}{1-\alpha t}, \tag{11}$$

where  $b, c$ , and  $\alpha$  are constants with  $b, c$ , and  $\alpha > 0$ .

By introducing the dimensionless functions  $f, g$ , and  $\theta$ , and the similarity variable  $\eta$ ,

$$\eta = \sqrt{\frac{b}{v(1-\alpha t)}}y, \psi = \sqrt{\frac{bv}{(1-\alpha t)}}xf(\eta), \omega = \sqrt{\frac{b^3}{v(1-\alpha t)^3}}xg(\eta), \theta(\eta) = \frac{T - T_\infty}{T_w - T_\infty}, \tag{12}$$

where  $\psi(x, y)$  is a stream function that is defined as  $u = \partial\psi/\partial y$  and  $v = -\frac{\partial\psi}{\partial x}$ , which both satisfies the mass conservation in Equation (1) and uses the dimensionless functions in Equation (12), we get the following equations.

$$\left(\frac{(1-\phi)^{-2.5} + K}{\beta}\right) f''' + f f'' - f'^2 - A\left(f' + \frac{\eta}{2} f''\right) + \frac{K B}{\beta} g' - (M + kp) f' = 0, \tag{13}$$

$$\left(\frac{(1-\phi)^{-2.5} + \frac{1}{2}K}{\beta}\right) g'' + f g' - f' g - A\left(\frac{3}{2}g + \frac{\eta}{2}g'\right) - \frac{K}{\beta}(2g + f'') = 0, \text{ and} \tag{14}$$

$$\left(L + \frac{4R}{3H}\right) \theta'' + Pr(f\theta' - f'\theta) - A Pr\left(\theta + \frac{\eta}{2}\theta'\right) = 0. \tag{15}$$

The boundary condition (5) is calculated in Equation (16).

$$f(0) = Sw, f'(0) = 1, g(0) = -nf''(0), \theta(0) = 1, f(\infty) = 0, g(\infty) = 0, \theta(\infty) = 0, \tag{16}$$

where

$$\beta = \left(1 - \phi + \phi \frac{\rho_s}{\rho_f}\right), H = \left(1 - \phi + \phi \frac{(\rho C_p)_s}{(\rho C_p)_f}\right), B = \frac{\nu(1-at)}{b_j}, L = \frac{\left(\frac{k_{nf}}{k_f}\right)}{H}, A = \frac{b}{a}, M = \frac{\sigma B^2(1-at)}{b\rho_f}, kp = \frac{\nu(1-at)}{bk_p}, K = \frac{k^*}{\mu}, R = \frac{4\sigma T_\infty^3}{\alpha^*k_f}, Pr = \frac{\nu_f(\rho C_p)_f}{k_f}.$$

### 3. Solutions and Results

#### 3.1. Steady Weak Concentration Boundary Layer

For the steady weak concentration boundary layer, we considered the unsteadiness parameter (A) = 0 and n = 0.5. Thus, Equations (13)–(15) became the equations below.

$$\left(\frac{(1-\phi)^{-2.5} + K}{\beta}\right) f''' + f f'' - f'^2 + \frac{K B}{\beta} g' - (M + kp)f' = 0, \tag{17}$$

$$\left(\frac{(1-\phi)^{-2.5} + \frac{1}{2}K}{\beta}\right) g'' + f g' - f' g - \frac{K}{\beta}(2g + f'') = 0, \text{ and} \tag{18}$$

$$\left(L + \frac{4R}{3H}\right) \theta'' + Pr(f\theta' - f'\theta) = 0. \tag{19}$$

The boundary condition (16) became Equation (20).

$$f(0) = Sw, f'(0) = 1, g(0) = -\frac{1}{2}f''(0), \theta(0) = 1, \\ f(\infty) = 0, g(\infty) = 0, \theta(\infty) = 0. \tag{20}$$

#### 3.1.1. Exact Solution of the Momentum Boundary Layer Problem

In this section, general solutions for Equations (17) and (18) are suggested in the form below.

$$f(\eta) = Sw + \frac{1}{m}(1 - e^{-m\eta}) \text{ and } g(\eta) = \frac{m}{2}e^{-m\eta}, \tag{21}$$

which are satisfied by the following conditions.

$$f(0) = Sw, f'(0) = 1, g(0) = -\frac{1}{2}f''(0), \theta(0) = 1, \tag{22}$$

$$f(\infty) = 0, g(\infty) = 0, \theta(\infty) = 0.$$

Upon substituting Equation (21) into Equations (17) and (18), and using the boundary conditions from Equation (22), we get the following equation.

$$m = \frac{\beta(1 - \phi)^{2.5}}{2(1 + \frac{1}{2}K(1 - \phi)^{2.5})} \left\{ Sw + \sqrt{(Sw)^2 + \frac{4(1 + \frac{1}{2}K(1 - \phi)^{2.5})(1 + M + kp)}{\beta(1 - \phi)^{2.5}}} \right\}. \tag{23}$$

Therefore, the linear velocity and angular velocity components take the form below.

$$u = (bx e^{-m\eta}), v = -\sqrt{bv_f} [Sw + \frac{1}{m}(1 - e^{-m\eta})]. \tag{24}$$

### 3.1.2. Exact Solution of the Momentum Boundary Layer Problem

By substituting Equation (19) into Equation (21), one can obtain the following ordinary differential equation.

$$\theta'' + \left( \frac{3HPr}{4R + 3HL} \right) \left[ (Sw + \frac{1}{m}(1 - e^{-m\eta}))\theta' - (e^{-m\eta})\theta \right] = 0, \tag{25}$$

with boundary conditions that are given by the following equation.

$$\theta(0) = 1, \theta'(\infty) = 0. \tag{26}$$

Equation (25) is a homogenous linear ordinary differential of the second order with a variable coefficient, which can be solved by introducing the change variable.

$$\varepsilon = -\lambda \frac{e^{-m\eta}}{m^2}, \tag{27}$$

where  $\lambda = \left( \frac{3HPr}{4R + 3HL} \right)$ . Equation (25) can then be written as below.

$$\varepsilon \frac{d^2\theta}{d\varepsilon^2} + [1 - \zeta - \varepsilon] \frac{d\theta}{d\varepsilon} + \theta = 0, \tag{28}$$

where  $\zeta = \frac{\lambda}{m^2}(1 + m Sw)$ , with the following boundary conditions.

$$\theta\left(\frac{\lambda}{m^2}\right) = 1 \text{ and } \theta'(\infty) = 0. \tag{29}$$

Equation (28) is similar to Kummer's differential equation, which has a Kummer confluent hypergeometric function, 1F1, as a solution.

$$\theta(\varepsilon) = \left(-\frac{\varepsilon m^2}{\lambda}\right)^\zeta \frac{1F1(\zeta - 1; \zeta + 1; -\varepsilon)}{1F1(\zeta - 1; \zeta + 1; -\frac{\lambda}{m^2})}. \tag{30}$$

The solution of Equation (30) in terms of the similarity variable ( $\eta$ ) can be found as described below.

$$\theta(\eta) = (e^{-m\eta})^\zeta \frac{1F1(\zeta - 1; \zeta + 1; -\varepsilon)}{1F1\left(\zeta - 1; \zeta + 1; -\frac{\lambda}{m^2}\right)}. \tag{31}$$

In addition, the surface temperature gradient is described below.

$$\theta'(0) = -(m\zeta) + \left(\frac{\lambda(\zeta - 1)}{m(\zeta + 1)}\right) \frac{1F1\left(\zeta; \zeta + 2; -\frac{\lambda}{m^2}\right)}{1F1\left(\zeta - 1; \zeta + 1; -\frac{\lambda}{m^2}\right)}. \tag{32}$$

### 3.2. Unsteady Weak Concentration Boundary Layer

The equations for the unsteady case at  $n = 0.5$ , Equations (13)–(15), and the boundary conditions, Equation (16), are solved numerically. In order to solve this system, we first need to find the missing initial conditions  $f''(0)$ ,  $g'(0)$ , and  $\theta'(0)$  by constructing a program for the system as an initial value problem with the missing initial conditions. In order to solve this system, we have to suggest a proper value of  $\eta \rightarrow \infty''\eta_\infty''$ . Following this, the missing and necessary values are calculated, using the root technique, by the code. Once the values of  $f''(0)$ ,  $g'(0)$ , and  $\theta'(0)$  have no change with an increase of  $\eta \rightarrow \infty$  (i.e., the boundary conditions  $f'(\eta_\infty) = 0$ ,  $g(\eta_\infty) = 0$ ,  $\theta'(\eta_\infty) = 0$  are satisfied at the suggested value of  $\eta \rightarrow \infty$ ), the system is ready to be solved, using the classical Runge–Kutta method from the fourth order with a step size of  $\Delta\eta = 0.01$ . To support the steady case results that were obtained by this method, the values in Table 2 are compared with the results for  $-C_f\sqrt{R_x}$  and  $g'(0)$ . The numerical solution was reported in Ezzah et al. [26] and the exact solution was obtained in this study.

**Table 2.** Comparison of  $-C_f\sqrt{R_x}$  and  $-g'(0)$  for several values of the suction parameter ( $Sw$ ) at the unsteadiness parameter ( $A$ ) = radiation parameter ( $R$ ) = 0,  $n = 0.5$ , nanoparticle concentration ( $\phi$ ) = 0.1 and the material parameter ( $K$ ) = 2, magnetic field parameter ( $M$ ) = 0.1, permeability of the porous medium parameter ( $kp$ ) = 0.1.

Parameter	Present Results				Ezzah [26]	
	Exact Solution		Numerical Solution			
$Sw$	$-C_f\sqrt{R_e}$	$-g'(0)$	$-C_f\sqrt{R_e}$	$-g'(0)$	$-C_f\sqrt{R_e}$	$-g'(0)$
2	3.9182	1.9190	3.9182	1.9190	3.9183	1.9191
3	5.27412	3.4770	5.27412	3.4770	5.2741	3.4770

## 4. Physical Aspect of the Problem

For certain important scientific purposes, it is useful to investigate the flow characteristics. The functions  $f''(0)$ ,  $g'(0)$ , and  $\theta'(0)$  allow us to determine the skin friction coefficient, the dimensionless couple stress, and the Nusselt number, which indicate the surface shear stress, the couple stress, and the rate of heat transfer, respectively. It is useful to mention the final quality of the surface that is controlled by the surface shear stress and couple stress. In addition, hardness, flexibility, and ductility are important mechanical properties of the surface and depend on the rate of heat transfer from the hot surface (the cooling rate).

### 4.1. Surface Shear Stress

The shear stress is defined below.

$$\tau_w = [(\mu_{nf} + k^*) \frac{\partial u}{\partial y} + k^* \omega]. \tag{33}$$

The local skin friction is defined below.

$$C_f = \frac{2\tau_w}{\rho_{nf}U_w^2} = \frac{2}{\sqrt{R_e}} \left( \frac{1}{\beta(1-\phi)^{2.5}} + \frac{K(1-n)}{\beta} \right) f''(0). \tag{34}$$

### 4.2. Surface Couple Stress

$$M_w = \gamma_{nf} \left[ \frac{\partial \omega}{\partial y} \right]. \tag{35}$$

The dimensionless couple stress is defined below.

$$M_x = \frac{2M_w}{\rho_{nf}v_{nf}U_w} = \left(2 + \frac{K(1-\phi)^{2.5}}{2}\right)g'(0). \tag{36}$$

### 4.3. Surface Heat Flux

$$q_w = -k_{nf}\left[\frac{\partial T}{\partial y}\right]. \tag{37}$$

The local Nusselt number is defined below.

$$Nu = \frac{xq_w}{k_f(T_w - T_\infty)} = -\frac{k_{nf}}{k_f}\left[\sqrt{Re}\theta'(0)\right]. \tag{38}$$

## 5. Discussion

The following discussion is based upon a numerical solution—supported by a solution form that was obtained for the nonlinear system—describing the micropolar nanofluid boundary layer over a moving flat surface, which is an emulation of the cooling process. The model considers the steady and unsteady boundary layer, which contains Cu (Copper) and is subjected to an external magnetic field, thermal radiation, and suction through porous media. The linear and angular velocities, along with the temperature profiles, are plotted and presented in Figures 2–8. In addition, the values of the local skin friction, couple stress, and local Nusselt number for Cu particles are presented in Tables 2 and 3.

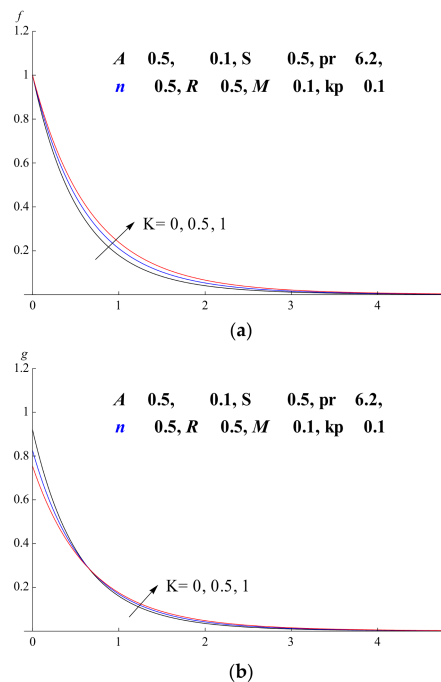


**Figure 2.** Influence of the material parameter ( $K$ ). (a) Velocity profile and (b) angular velocity profile.

### 5.1. Material Parameter

Newtonian or non-Newtonian fluids depend on the ratio between the vortex viscosity and the dynamics viscosity, which is called the material parameter ( $K$ ), so that  $K = 0$  represents Newtonian fluids when there is no vortex viscosity. Figure 2a,b characterize the linear and angular velocity profiles under the variation of the material parameter. We can see that the linear velocity increases when this parameter rises but the angular velocity decreases near the surface—because of microrotation—before

reversing and increasing farther from the surface. The changes in the surface skin friction, couple stress, and Nusselt number are presented in Tables 3 and 4, and physically indicate the surface shear stress, the couple stress, and the rate of heat transfer. In general, it is observed that the presence of the viscosity vortex ( $K \neq 0$ ), due to the microstructures microrotation, increases near the surface shear stress and the rate of heat transfer. Physically, the weak angular velocity near the surface resulted from a weak concentration of the microstructures.

**Table 3.** Values of  $-f''(0)$ ,  $-g'(0)$ , and  $-\theta'(0)$  for the steady case [ $A = 0$ ] at  $R = 1$ , Prandtl number ( $Pr$ ) = 6.2,  $M = 0.1$ ,  $kp = 0.1$ .

K	$Sw$	$-\phi$	$f''(0)$	$-g'(0)$	$-\theta''(0)$	$C_f\sqrt{Re}$	$-Nul\sqrt{Re}$	$M_x$	
0	-0.5	0.1	4.038346	0.979447	0.531071	-8.076692	0.531071	-1.958894	
		0.1	3.584031	0.712813	0.518383	-7.189817	0.690297	-1.699500	
		0.2	3.130794	0.576239	0.564942	-4.220449	0.986223	-1.152478	
	0	0.0	0.0	4.464803	1.728692	0.924024	-13.39440	0.924024	-4.321730
		0.1	0.1	3.913861	1.421675	1.020822	-5.672146	1.359363	-2.843350
		0.2	0.2	3.378040	0.990240	1.344222	-5.857106	2.346619	-2.263903
	0.5	0.5	0.0	4.936295	3.625016	1.828576	-9.872590	1.828576	-7.250032
			0.1	4.274045	2.593231	1.895725	-8.574034	2.524416	-6.182824
			0.2	3.644810	1.769211	2.522203	-4.913365	4.403029	-3.538422
0.5	-0.5	0.0	3.405583	0.803944	0.522100	-10.21674	0.522100	-2.009860	
		0.1	3.124187	0.686680	0.551381	-4.527714	0.734239	-1.373360	
		0.2	2.814292	0.574242	0.594486	-4.879636	1.037798	-1.312841	
	0	0.0	0.0	3.743495	1.450575	0.992598	-7.486990	0.992598	-2.901150
		0.1	0.1	3.400468	1.189547	1.054966	-6.821577	1.404831	-2.836137
		0.2	0.2	3.030169	0.926740	1.126033	-4.084802	1.965724	-1.853480
	0.5	0.5	0.0	4.141100	2.661302	1.888458	-12.42330	1.888458	-6.653255
			0.1	3.715203	2.044583	1.944352	-5.384242	2.589170	-4.089166

**Table 4.** Values of  $-f''(0)$ ,  $-g'(0)$ , and  $-\theta'(0)$  for the unsteady case [ $A = 1$ ] at  $R = 1$ ,  $Pr = 6.2$ ,  $M = 0.1$ ,  $kp = 0.1$ .

K	$Sw$	$\phi$	$-f''(0)$	$-g'(0)$	$-\theta''(0)$	$C_f\sqrt{Re}$	$-Nul\sqrt{Re}$	$M_x$	
0	-0.5	0.0	4.190553	3.102011	1.339903	-8.381106	1.339903	-6.204022	
		0.1	3.717099	2.476667	1.365301	-7.456761	1.818084	-5.904910	
		0.2	3.245327	1.915456	1.393946	-4.374844	2.433422	-3.830912	
	0	0.0	0.0	4.613003	4.263178	1.777243	-13.83900	1.777243	-10.65794
		0.1	0.1	4.043774	3.276003	1.810996	-5.860422	2.411588	-6.552006
		0.2	0.2	3.490167	2.440392	2.177493	-6.051520	3.801266	-5.579264
	0.5	0.5	0.0	5.079028	5.919060	2.410378	-10.15805	2.410378	-11.83812
			0.1	4.399817	4.367775	2.450397	-8.826341	3.263038	-10.41372
			0.2	3.753898	3.128262	3.065966	-5.060420	5.352281	-6.256524
0.5	-0.5	0.0	3.6246638	2.481260	1.366782	-10.87399	1.366782	-6.203150	
		0.1	3.308656	2.072541	1.386910	-4.795055	1.846860	-4.145082	
		0.2	2.965490	1.670736	1.410602	-5.141795	2.462499	-3.819664	
	0	0.0	0.0	3.958321	3.301533	1.810306	-7.916642	1.810306	-6.603066
		0.1	0.1	3.5798703	2.679505	1.837633	-7.181471	2.447059	-6.388520
		0.2	0.2	3.177986	2.096067	1.869445	-4.284066	3.263504	-4.192134
	0.5	0.5	0.0	4.330744	4.434499	2.446977	-12.99223	2.446977	-11.08624
			0.1	3.878216	3.489879	2.479820	-5.620487	3.302219	-6.979758
			0.2	3.408446	2.6443808	2.517496	-5.909826	4.394812	-6.045627

### 5.2. Steady/Unsteady Boundary Layer

The value of the unsteadiness parameter ( $A$ ) indicates the type of motion such that for  $A = 0$ , the problem is reduced to the steady case, and  $A \neq 0$  indicates the unsteady motion. Moreover, the positive sign of this unsteadiness parameter indicates accelerated motion and the negative sign indicates deceleration. Figure 3a,b indicate the effect of the unsteadiness parameter on the linear and

angular velocities. It is observed that increasing this parameter leads to a decrease in the linear and angular velocities when it is close to the surface. This effect is reversed when it is far away from the surface. Figure 3c indicates that the unsteadiness parameter has a finite effect on the boundary layer temperature. It is important to mention that only the steady motion, indicated by a black line, is plotted in Figure 3a–c. On the other hand, Tables 3 and 4 present a comparison of the physical characteristics of the steady and unsteady boundary layers through the values of the surface skin friction, couple stress, and Nusselt number. In the case of unsteady motion, the surface skin friction value is larger for Newtonian fluids ( $K = 0$ ) than it is for non-Newtonian fluids ( $K \neq 0$ ). This means that the skin friction is more affected by Newtonian fluids than by non-Newtonian fluids. Additionally, in the case of unsteady motion, we observe the same effect for the couple stress and the local Nusselt number. It is observed that increasing the surface heat flux, caused by the increase of the Nusselt number, will accelerate the rate of cooling.

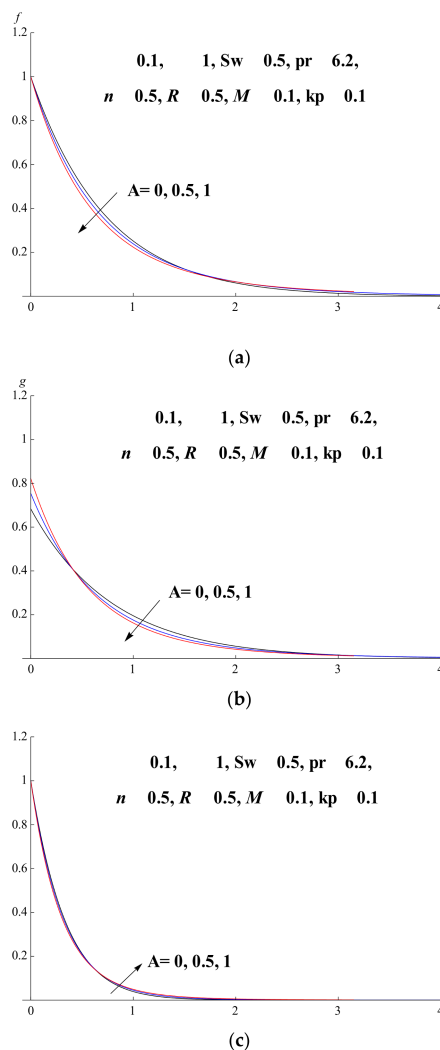


**Figure 3.** Influence of the unsteadiness parameter ( $A$ ). (a) Velocity profile, (b) angular velocity profile, and (c) temperature profile.

### 5.3. Nanoparticle Concentration

The ratio  $\phi$  represents the nanoparticle concentration within the fluid. It is clear that for  $\phi = 0$ , the problem is converted to the regular micropolar fluid. This implies that this ratio controls the dynamic viscosity and the thermal conductivity of the fluid, such that the linear velocity of the flow increases by increasing the nanoparticle concentration (see Figure 4a). On the other hand, Figure 4b

indicates that the presence of the nanoparticles increases the angular velocity when it is close to the surface. As a result of presence of the nanoparticles, Figure 4c indicates that the boundary layer temperature increases when the thermal conductivity grows. Table 3 illustrates the influence of the nanoparticle concentration on the surface skin friction, couple stress, and Nusselt number. It is observed that the nanoparticle concentration is more effective on the skin friction when there is no suction effect than it is when there is a suction effect. Additionally, it is clear that the nanoparticle concentration is more effective on the couple shear stress when there is a suction effect than it is when there is no suction effect. Moreover, according to the steadiness parameter and the material parameter, the rate of heat transfer increases when the local Nusselt number rises. In general, increasing the skin friction or the couple stress has a negative effect on the quality of the outer surface of the plate. When the Nusselt number increases, the rate of heat transfer from the surface rises, which has a positive effect on certain of the mechanical properties, such as hardness and strength.

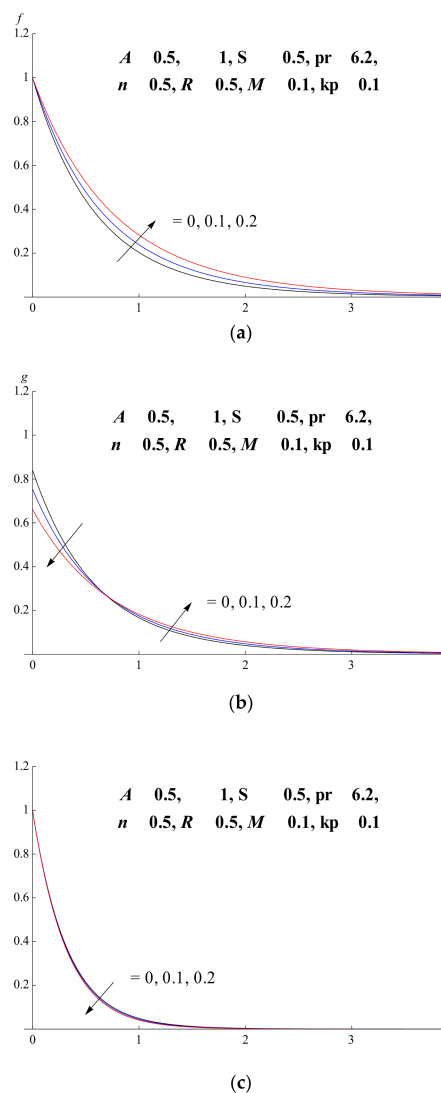


**Figure 4.** Influence of the nanoparticle concentration. (a) Velocity profile, (b) angular velocity profile, and (c) temperature profile.

#### 5.4. Suction Parameter Effect

Additionally, the effect of the suction parameter ( $Sw$ ) on the velocities and the temperature are presented in Figure 5a–c, respectively. Figure 5a,b indicate that the linear and angular velocities

decrease with increasing values of  $Sw$ . The fluid velocities are found to decrease with the increase in  $Sw$ , which means that suction causes a dragging force that decreases the fluid velocity in the boundary layer. Figure 5c indicates that the temperature in the boundary layer decreases with increasing values of  $Sw$ , which causes a decrease in the rate of heat transfer from the fluid to the surface. The thermal boundary layer is thinner in the case of suction.

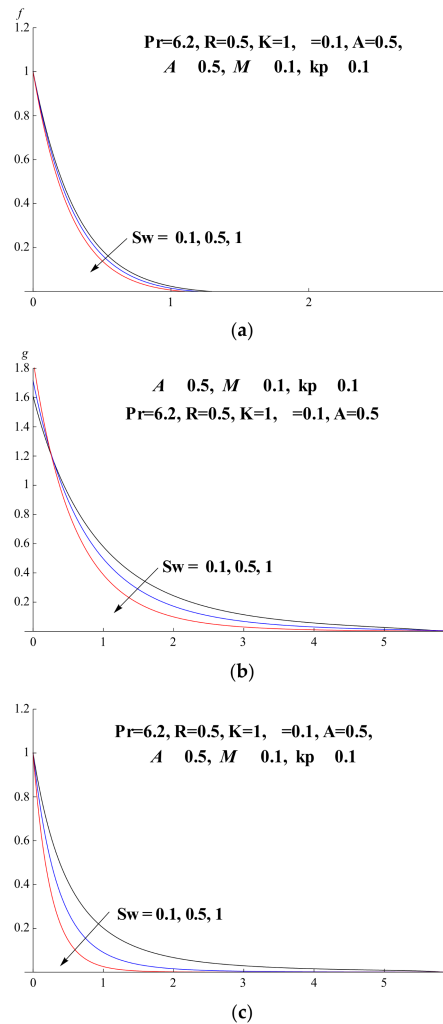


**Figure 5.** Influence of suction parameter ( $Sw$ ). (a) Velocity profile, (b) angular velocity profile, and (c) temperature profile.

### 5.5. Permeability Effect

Figure 6a depicts the effect of the permeability of the porous medium parameter ( $kp$ ) on the velocity distribution profile. It is clear that as  $kp$  increases, the linear velocity decreases along the boundary layer thickness. This is expected, since the holes of the porous medium become larger. Figure 6b indicates the influence of  $kp$  on the angular velocity distribution. It is obvious that as  $kp$  increases, the angular velocity decreases.

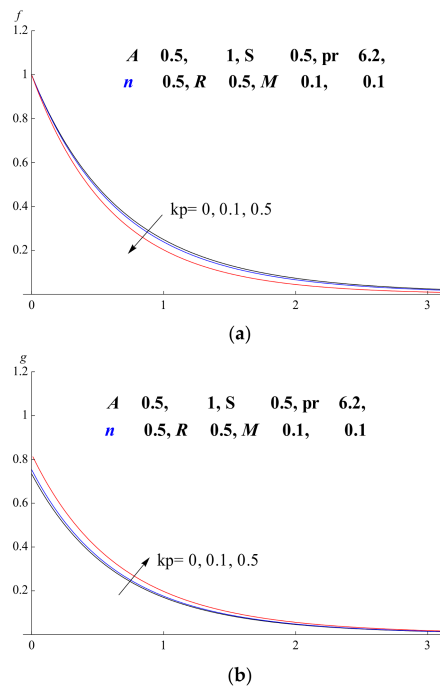


**Figure 6.** Influence of the porous media parameter ( $kp$ ). (a) Velocity profile and (b) Angular velocity profile.

5.6. Magnetic–Radiation Effect

Figure 7a,b indicate the effect of the magnetic field parameter ( $M$ ) on the velocities. With the increase of  $M$ , the linear velocity and the angular velocity of the flow decrease. Figure 8 illustrates the temperature profiles for different values of the radiation parameter ( $R$ ). The figure indicates that as the value of  $R$  increases, the temperature profiles increase.

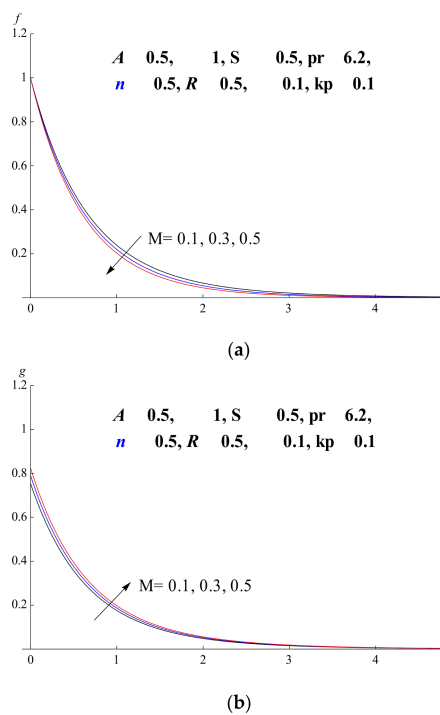


**Figure 7.** Influence of the magnetic parameter ( $M$ ). (a) Velocity profile and (b) angular velocity profile.

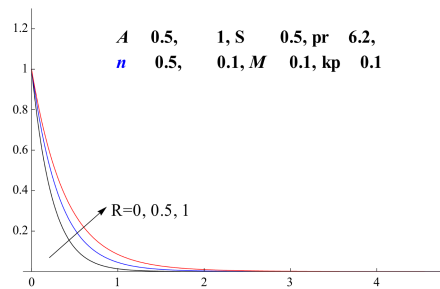


Figure 8. Temperature profile with increasing radiation parameter ( $R$ ).

## 6. Conclusions

The heat transfer rate decreases in the case of the unsteady boundary layer when compared to the case of the steady boundary layer. The rate of heat transfer increases more for non-Newtonian fluids than it does for Newtonian fluids. Furthermore, Newtonian fluids are more effective for increasing the surface shear stress and couple stress than non-Newtonian fluids. Moreover, the presence of nanoparticles increases the rate of heat transfer for the non-Newtonian boundary layer when compared to Newtonian fluids. Lastly, the rate of heat transfer, the surface shear stress, and the couple shear stress decrease during the suction process.

**Acknowledgments:** The authors would like to express their very sincere thanks to the editor and the reviewers for their valuable comments and suggestions.

**Author Contributions:** Kamal Raslan and Selim Mohamadain suggested the problem and Mohamed Abdel-wahed with Elsayed M. Abdel-aal analyzed the data and Elsayed M. Abdel-aal wrote it.

**Conflicts of Interest:** The authors declare no conflict of interest.

## Abbreviations

$x, y$	Cartesian coordinate system
$b$ and $c$	Constants
$u, v$	Velocity components along the $x$ -, $y$ -directions
$\omega$	Angular velocity
$t$	Time
$\psi(x, y)$	The stream function
$Uw, Vw$	Velocity of the stretching sheet along $x$ - and $y$ -directions
$T$	Fluid temperature
$n$	boundary parameter
$k^*$	vortex viscosity
$K_p$	Porous medium parameter
$Sw$	Suction parameter
$K$	Material parameter
$B_0$	Magnetic field
$A$	Unsteadiness parameter
$q_r$	Radiative heat flux
$\alpha^*$	Mean absorption coefficient
$j$	Micro-inertia per unit mass
$Pr$	Prandtl number
$R$	Radiation parameter
$f, g$	Dimensionless components of velocities
$\tau_w$	Shear stress
$C_f$	Skin friction
$M_x$	Dimensionless couple stress
$Nu$	Nusselt number
$\rho$	Density of the fluid
$\gamma$	Spin gradient viscosity

$\sigma$	Stefen–Boltzmann constant
$\alpha_{nf}$	thermal diffusivity of the nanofluid
$k$	Thermal conductivity
$\mu$	Dynamic viscosity
$\nu$	kinematic viscosity
$\eta$	Similarity variable
$\phi$	Nanoparticles concentration
$\theta$	Dimensionless temperature.

**Subscripts**

$f$	Fluid phase
$nf$	Nanofluid
$s$	Solid particles
$w$	Condition of the wall
$\infty$	Ambient condition

**References**

1. Elbashbeshy, E.M.A.; Emam, T.G.; Abdel-Wahed, M.S. Effect of heat treatment process with a new cooling medium (nanofluid) on the mechanical properties of an unsteady continuous moving cylinder. *J. Mech. Sci. Technol.* **2013**, *27*, 3843–3850. [[CrossRef](#)]
2. Das, S.K.; Choi, S.U.S.; Yu, W.; Pradeep, T. *Nanofluids: Science and Technology*; John Wiley & Sons: Hoboken, NJ, USA, 2007; ISBN 978-0-470-07473-2.
3. Choi, S.U.S.; Eastman, J.A. Enhancing conductivity of fluids with nanoparticles. *ASME Fluid Eng. Div.* **1995**, *231*, 99–105.
4. Sheikholeslami, M.; Hayat, T.; Alsaedi, A. MHD free convection of Al<sub>2</sub>O<sub>3</sub>–water nanofluid considering thermal radiation: A numerical study. *Int. J. Heat Mass Transf.* **2016**, *96*, 513–524. [[CrossRef](#)]
5. Azizah, M.; Syakila, A.; Pop, I. Flow and heat transfer over an unsteady shrinking sheet with suction in nanofluids. *Int. J. Heat Mass Transf.* **2011**, *55*, 1888–1897.
6. Hamad, M. Analytical solution of natural convection flow of a nanofluid over a linearly stretching sheet in the presence of magnetic field. *Int. Commun. Heat Mass Transf.* **2011**, *38*, 487–492. [[CrossRef](#)]
7. Nazar, R.; Tham, L.; Pop, I. Mixed convection boundary layer flow from a horizontal circular cylinder embedded in a porous medium filled with a nanofluid. *Transp. Porous Med.* **2011**, *86*, 517–536. [[CrossRef](#)]
8. Yacob, N.A.; Ishak, A.; Nazar, R.; Pop, I. Boundary layer flow past a stretching/shrinking surface beneath an external uniform shear flow with a convective surface boundary condition in a nanofluid. *Nanoscale Res. Lett.* **2011**, *6*, 1–7. [[CrossRef](#)] [[PubMed](#)]
9. Elbashbeshy, E.M.A.; Emam, T.G.; Abdel-Wahed, M.S. Effect of magnetic field on flow and heat transfer of a nanofluid over an unsteady continuous moving surface in the presence of suction/injection. *Int. J. Appl. Math.* **2012**, *14*, 436–442.
10. Qasim, M.; Khan, Z.; Lopez, R.; Khan, W. Heat and mass transfer in nanofluid thin film over an unsteady stretching sheet using Buongiorno’s model. *Eur. Phys. J. Plus* **2016**, *131*, 16. [[CrossRef](#)]
11. Anbuhezian, N.; Srinivasan, K.; Chandrasekaran, K.; Kandasamy, R. Thermophoresis and Brownian motion effects on boundary layer flow of nanofluid in presence of thermal stratification due to solar energy. *Appl. Math. Mech.* **2012**, *33*, 765–780. [[CrossRef](#)]
12. Elbashbeshy, E.M.A.; Emam, T.G.; Abdel-Wahed, M.S. Flow and heat transfer over a moving surface with non-linear velocity and variable thickness in a nanofluid in the presence of thermal radiation. *Can. J. Phys.* **2013**, *91*, 699–708.
13. Elbashbeshy, E.M.A.; Emam, T.G.; Abdel-Wahed, M.S. An exact solution of boundary layer flow over a moving surface embedded into a nanofluid in the presence of magnetic field and suction/injection. *Heat Mass Transf.* **2014**, *50*, 57–64. [[CrossRef](#)]
14. Elbashbeshy, M.A.; Emam, T.G.; Abdel-Wahed, M.S. The effect of thermal radiation and heat generation on the mechanical properties of unsteady continuous moving cylinder in a nanofluid in the presence of suction or injection. *Therm. Sci.* **2015**, *19*, 1591–1601. [[CrossRef](#)]
15. Abdel-wahed, M.S.; Elbashbeshy, E.M.A.; Emam, T.G. Flow and heat transfer over a moving surface with non-linear velocity and variable thickness in a nanofluid in the presence of Brownian motion. *Appl. Math. Comput.* **2015**, *254*, 1591–1601. [[CrossRef](#)]

16. Yain, Y.; Amin, N.; Pop, I. Unsteady boundary layer flow of a micropolar fluid near rear stagnation point of a plane surface. *Int. J. Therm. Sci.* **2003**, *42*, 995–1001.
17. Sandeep, N.; Sulochana, C. Dual solution for unsteady mixed convection flow of MHD micropolar fluid over a stretching/shrinking sheet with non-uniform heat source/sink. *Eng. Sci. Technol.* **2015**, *18*, 738–745. [[CrossRef](#)]
18. Abo-Eldahab, E.M.; El Aziz, M.A. Flow and heat transfer in a micropolar fluid past a stretching surface embedded in a non-Darcian porous medium with uniform free stream. *Appl. Math. Comput.* **2005**, *162*, 881–899. [[CrossRef](#)]
19. Rahman, M.; Sultana, T. Radiative Heat transfer flow of micropolar fluid with variable heat flux in a porous medium. *Nonlinear Anal. Model. Control* **2008**, *13*, 17–87.
20. Ishak, A.; Nazar, R.; Pop, I. Heat transfer over a stretching surface with variable heat flux in micropolar fluids. *Phys. Lett. A* **2007**, *372*, 559–561. [[CrossRef](#)]
21. Khedr, M.E.M.; Chamkha, A.J.; Bayomi, M. MHD flow of a micropolar fluid past a stretched permeable surface with heat generation or absorption. *Nonlinear Anal. Model. Control* **2009**, *14*, 27–40.
22. Rahman, M.; El-tayeb, A.; Rahman, S.M.M. Thermo-micropolar fluid flow along a vertical permeable plate with uniform surface heat flux in the presence of heat generation. *Therm. Sci.* **2009**, *13*, 23–36. [[CrossRef](#)]
23. Saad, A.A.; Abdel-Wahed, M.S. Heat transfer over unsteady moving surface with heat generation and thermal radiation in micropolar fluid in the presence of suction/injection. *Int. J. Energy Technol.* **2011**, *3*, 1–7.
24. L-Arabawy, H.A.M.E. Effects of suction/injection on the flow of micropolar fluid past a continuously moving plate in the presence of radiation. *Int. J. Heat Mass Transf.* **2003**, *46*, 1471–1477. [[CrossRef](#)]
25. Hussain, S.T.; Nadeem, S.; Haq, R.U. Model-based analysis of micropolar nanofluid flow over a stretching surface. *Eur. Phys. J. Plus* **2014**, *129*, 161. [[CrossRef](#)]
26. Ezzah, L.A.; Syakila, A.; Pop, I. Flow over a permeable stretching sheet in micropolar nanofluids with suction. *AIP Conf. Proc.* **2014**, *1605*, 428–433.
27. Turkyilmazoglu, M. Flow of a micropolar fluid due to a porous stretching sheet and heat transfer. *Int. J. Non-Linear Mech.* **2016**, *83*, 59–64. [[CrossRef](#)]
28. Mabood, F.; Ibrahim, S.M.; Rashidi, M.M.; Shadloo, M.S. Giulio Lorenzini, Nonuniform heat source/sink and Soret effects on MHD non-Darcian convective flow past a stretching sheet in a micropolar fluid with radiation. *Int. J. Heat Mass Transf.* **2016**, *93*, 674–682. [[CrossRef](#)]
29. Ramzan, M.; Farooq, M.; Hayat, T.; Chung, J.D. Radiative and Joule heating effects in the MHD flow of a micropolar fluid with partial slip and convective boundary condition. *J. Mol. Liq.* **2016**, *221*, 394–400. [[CrossRef](#)]
30. Hsiao, K. Micropolar nanofluid flow with MHD and viscous dissipation effects towards a stretching sheet with multimedia feature. *Int. J. Heat Mass Transf.* **2017**, *112*, 983–990. [[CrossRef](#)]
31. Mahmood, A.; Chen, B.; Ghaffari, A. Hydromagnetic Hiemenz flow of micropolar fluid over a nonlinearly stretching/shrinking sheet: Dual solutions by using Chebyshev Spectral Newton Iterative Scheme. *J. Magn. Magn. Mater.* **2016**, *416*, 329–334. [[CrossRef](#)]
32. Borrelli, A.; Giancesio, G.; Patria, M.C. MHD orthogonal stagnation-point flow of a micropolar fluid with the magnetic field parallel to the velocity at infinity. *Appl. Math. Comput.* **2015**, *264*, 44–60. [[CrossRef](#)]
33. Abdel-Wahed, M.S. Lorentz force effect on mixed convection micropolar flow in a vertical conduit. *Eur. Phys. J. Plus* **2017**, *132*, 195. [[CrossRef](#)]
34. Abdel-wahed, M.S. Flow and heat transfer of a weak concentration micropolar nanofluid over steady/unsteady-moving surface. *Appl. Phys. A* **2017**, *123*, 195. [[CrossRef](#)]
35. Vo, T.Q.; Kim, B.H. Molecular Dynamics Study of Thermodynamic Properties of Nanoclusters for Additive Manufacturing. *Int. J. Precis. Eng. Manuf. Green Technol.* **2017**, *4*, 301–306. [[CrossRef](#)]
36. Vo, T.Q.; Park, B.; Park, C.; Kim, B. Nano-scale liquid film sheared between strong wetting surfaces: Effects of interface region on the flow. *J. Mech. Sci. Technol.* **2015**, *29*, 1681–1688. [[CrossRef](#)]
37. Priezjev, N.V. Molecular dynamics simulations of oscillatory Couette flows with slip boundary conditions. *Microfluid Nanofluid* **2013**, *14*, 225–233. [[CrossRef](#)]
38. Kim, B.H.; Beskok, A.; Cagin, T. Viscous heating in nanoscale shear driven liquid flows. *Microfluid Nanofluid* **2010**, *9*, 31–40. [[CrossRef](#)]
39. Rodriguez-Lopez, J.L.; Montejano-Carrizales, J.M.; Jose-Yacamán, M. Molecular dynamics study of bimetallic nanoparticles: The case of AuCu alloy clusters. *Appl. Surf. Sci.* **2003**, *219*, 56–63. [[CrossRef](#)]

40. Kim, B. Thermal resistance at a liquid–solid interface dependent on the ratio of thermal oscillation frequencies. *Chem. Phys. Lett.* **2012**, *554*, 77–81. [[CrossRef](#)]
41. Murad, S.; Puri, I.K. Molecular simulation of thermal transport across hydrophilic interfaces. *Chem. Phys. Lett.* **2008**, *467*, 110–113. [[CrossRef](#)]



© 2018 by the authors. Licensee MDPI, Basel, Switzerland. This article is an open access article distributed under the terms and conditions of the Creative Commons Attribution (CC BY) license (<http://creativecommons.org/licenses/by/4.0/>).